Stratospheric prediction in NWP models

Gregory L. Roff

Bureau of Meteorology, 150 Lonsdale Street
Melbourne, 3001, Australia
g.roff@bom.gov.au

ABSTRACT

The question asked here is "How well do current NWP models simulate the stratosphere when the polar vortex undergoes large changes?". To answer this question we compare the analyses and forecasts from the BAM, ECMWF, NCEP, NOGAPS and UKMO models during periods when the polar vortex is undergoing rapid changes during the southern hemisphere major sudden warming of 2002.

We have found that the BAM, ECMWF, NCEP, NOGAPS and UKMO NWP models have well correlated analyses over the period of our study when the vortex is quasi-stationary but that when the polar vortex is undergoing rapid changes these analyses are seen to have larger RMSE differences and to become less correlated. Also during these active periods the model analyses correlations with TOMS TCO decreases dramatically from the very high values found when the vortex is quiescent.

The forecasting ability of the BAM, ECMWF, NCEP and NOGAPS NWP models has been studied during this sudden warming and we find that if the vortex undergoes rapid changes after forecast initialization all the models have some degree of difficulty in capturing this event. There are certain verification days, common to all the forecast models, which the model forecasts have difficulty, and these errors are largest in the stratosphere. These characteristic errors were that the forecast vortex was seen to be: smaller; displaced westward; displaced poleward; have a faster easterly rotation of its orientation and to be more circular.

1 Introduction

Short-term stratospheric forecasts are an important tool for ozone and ultraviolet forecasting systems (eg Atkinson *et al.* 1997) as well as for aircraft flight planning for stratospheric observational campaigns (eg Tuck *et al.* 1989, 1997). These forecasts are also important because the stratospheric circulation can impact on the tropospheric circulation directly via the "downward control" mechanism (Haynes *et al.* 1991; Hartley *et al.* 1998) and indirectly by changes in the refraction of planetary waves dispersing upward from the troposphere (Hartmann *et al.* 2000; Shindell *et al.* 2001). Large changes in the strength and shape of the polar vortex have been shown to impact on the tropospheric circulation (Baldwin and Dunkerton 1999, 2001; Thompson *et al.* 2002) and so the ability to forecast accurately in the stratosphere is also beneficial to weather prediction ie tropospheric forecasting.

The wintertime extra-tropical stratospheric circulation is dominated by a quasi-stationary polar vortex, driven by relaxation toward radiative equilibrium. Variability in this circulation is largely due to low frequency interactions between the zonal flow and planetary-scale waves dispersing upward from the troposphere. However the corresponding tropospheric variability is driven by higher frequency rapidly evolving baroclinic waves. We thus expect better forecast skill in the stratosphere than the troposphere because of the formers low frequency variability. Indeed, Waugh *et al.* (1998) found that the forecasting performance at seven days in the stratosphere is comparable to three days in the troposphere. Waugh *et al.* (1998) also found large variability in stratospheric forecast skill at seven days, with poorer scores occurring when the vortex flow is rapidly

changing. Such rapid changes in the polar vortex occur during sudden warmings.

Sudden warmings are a breakdown or reversal, defining a minor or major warming respectively, of the polar vortex zonal-mean westerly wind accompanied by a rapid rise in polar temperature (Labitzke 1982; McIntyre 1982; Andrews *et al.* 1987) and are linked to the propagation from the troposphere to the stratosphere of large amplitude wave disturbances (Matsuno 1971) by means of wave-mean-flow interactions (Andrews 1985). Plots of timeseries of the 10 hPa BAM, ECMWF, NCEP, NOGAPS and UKMO analyses polar zonal mean geopotential height, temperature and zonal wind fields, overlayed with the corresponding TOMS Total Column Ozone (TCO) field, for the warming studied in this paper can be seen in Figure 1. These plots cover the

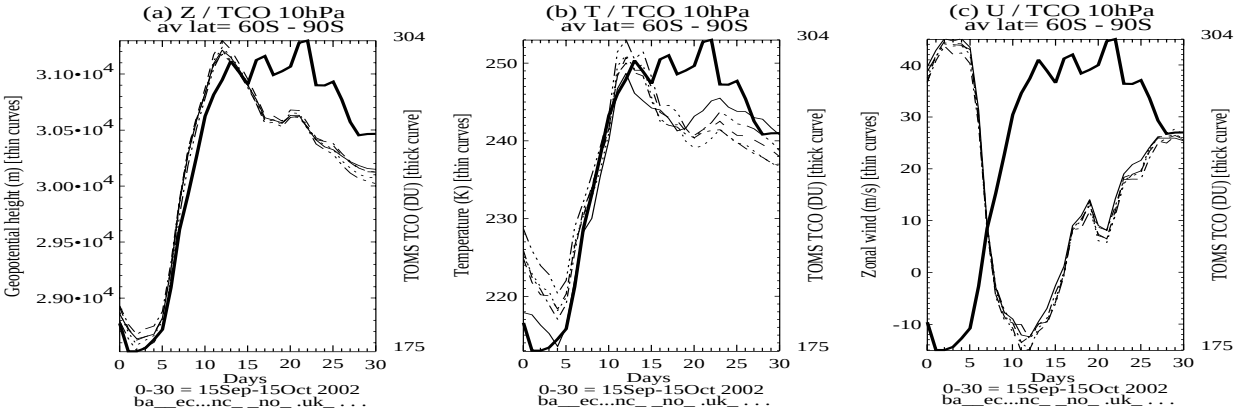

Figure 1: Timeseries of TOMS total column ozone (DU), thick curve, and BAM, ECMWF, NCEP, NOGAPS and UKMO analyses (a) geopotential height (m), (b) temperature (K) and (c) zonal wind (ms^{-1}) fields (thin curves, styles indicated) averaged over the polar region ($60^oS - 90^oS$) at 10 hPa for 15 September 2002 to 15 October 2002 (Days 0-30).

period 15 September 2002 to 15 October 2002 (referred to as Days 0-30 for this study). The rapid increase in TOMS TCO over the polar region can be seen to coincide with a sudden increase in geopotential height and temperature as well as a reversal of the zonal wind to easterlies. These dramatic changes in TOMS TCO and 10 hPa geopotential height, temperature and zonal wind (128 *DU*, 2770 *m*, 40 *K*, 60 ms^{-1}, respectively) occurred over an eight day period from 20-27 September (Days 5-12) with the vortex then attempting to re-establish itself, though the final state of the vortex is much weaker, having lower zonal winds and warmer temperatures, than its initial state.

Sudden warmings are relatively common in the northern hemisphere with a major warming occurring approximately every two years (Andrews *et al.* 1987). However the first recorded southern hemisphere major sudden warming occurred in September 2002 and is thought to have occurred due to pre-conditioning by earlier wave events from July to September (Baldwin *et al.* 2003; Simmons *et al.* 2003). Daily polar stereographic TOMS TCO plots from 15 September to 15 October covering this warming event can be seen in Figure2. The evolution of the vortex from a single, large, pole centred cell through the sudden warming split into two cells from 20-27 September (Days 5-12) and then the growth of a smaller, symmetric and pole centred vortex can be seen. This figure is discussed in detail in the next section.

These dramatic changes to the polar vortex are seen to occur over short time scales and thus provide an excellent test for short-term forecasting systems operating in the stratosphere since accurately predicting the stratospheric flow requires the structure of this polar vortex breakdown to be well simulated.

Stratospheric prediction studies have been made in the northern hemisphere (Miyakoda *et al.* 1970; Simmons and Strufing 1983; Mechoso *et al.* 1985; and Carver *et al.* 1994; Klinker 1994; Simmons 1994) and the southern hemisphere (Karoly *et al.* 1993; Bourke *et al.* 1995; Waugh *et al.* 1998; and Lahoz 1999). Stratospheric forecast skill has been found to increase by increasing the vertical resolution of the stratosphere and this higher

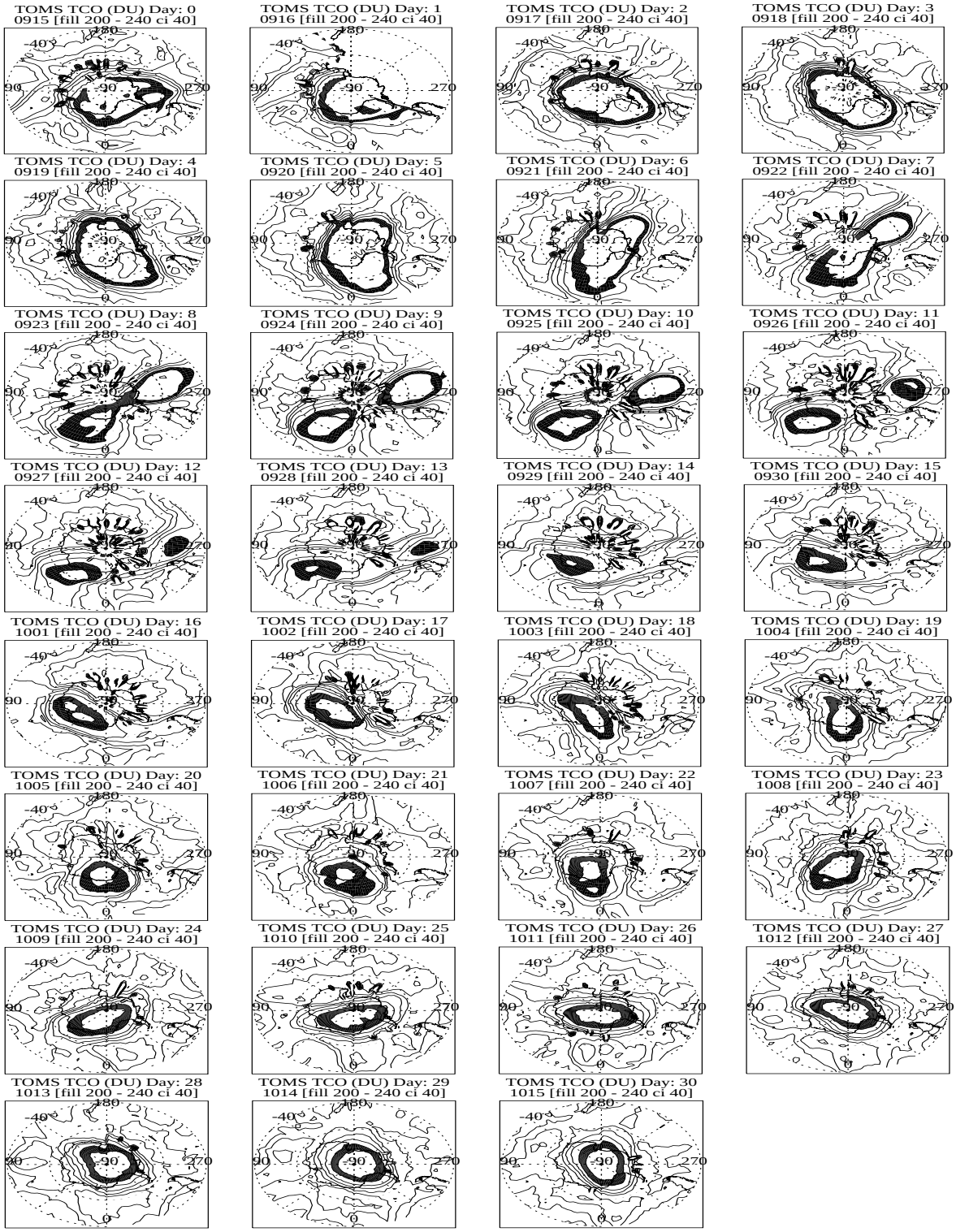

Figure 2: Daily southern hemisphere polar stereographic plots, for latitudes 40^oS *to* 90^oS*, of the TOMS total column ozone (DU) from 15 September 2002 to 15 October 2002 (Days 0-30). The contour interval is 40 DU, with shading between 200-240 DU, and the Greenwich Meridian is at the bottom with the* 40^oS *and* 60^oS *latitude circles marked.*

vertical resolution is needed in the stratosphere for better forecasting of tropospheric low-frequency variables. Similarly too low a rigid upper boundary or too coarse a vertical resolution in the stratosphere distorts the planetary waves in the troposphere (Tsuyuki 1994). Thus it would seem that numerical weather prediction (NWP) models with high model tops and high vertical resolution in the stratosphere should provide better stratospheric forecast skill. However Lahoz (1999) found that a model's skill in the lower stratosphere also depends on flow structure while the skill in the mid-troposphere was found to be independent of stratospheric representation. Waugh *et al.* (1998) found that the forecast vortex is weaker, less disturbed (closer to the pole and less elongated) and its orientation rotates faster than the corresponding analyses vortex. Consistent with this weakened forecast vortex, the minimum polar temperature and maximum zonal wind are also underestimated.

This paper reports on a WGNE project which aims to compare stratospheric predictability capabilities of present day NWP systems and their ability to capture polar vortex dynamics in both their analyses and forecasts. The NWP models we have data from are BAM, ECMWF, NCEP, NOGAPS and UKMO and colleagues who provided data for this study are listed in Table 1, along with the top data and model levels available and what forecasts were provided. Details of the models used to create these datasets are now discussed.

Model	Contact	Country	Data Top (hPa)	Model Top (hPa)	Forecasts
BAM	Gregory Roff	Australia,BMRC	10.0	10.0	5 day
ECMWF	Agathe Untch	EU,ECMWF	1.0	0.1	10 day
NCEP	Mark Iredell	USA,NCEP	7.0	1.0	10 day
NOGAPS	John McCormack	USA,NRL	10.0	1.0	5 day
UKMO	Adam Scaife	UK,UKMO	0.3	0.3	10 day[1]

Table 1: Experiment participants.([1] Forecasts did not arrive in time for this report.)

The Australian Bureau of Meteorology Research Centre's Atmospheric GCM, BAM[1], is a descendant of a spectral general circulation model first developed in the 1970's at BMRC (Bourke 1974, Bourke *et al.* 1977, McAvaney *et al.* 1978). Key documentation of the BMRC model is provided by Bourke (1988), Hart *et al.* (1988, 1990), Colman and McAvaney (1991), McAvaney *et al.* (1991) and Rikus (1991). The model was run with T239 resolution and 29 sigma levels in the vertical with a model top at 10 hPa and it has strong diffusion applied in the top levels which eliminates any spurious winds found here.

The ECMWF[2] model was run with triangular truncation of 511 with linear grid TL511 resolution in September 2002 and 60 hybrid eta-levels in the vertical up to 0.1 hPa and enhanced diffusion in the upper 13 levels.

The NOGAPS[3] model (Bayler and Lewitt, 1992; Goerss and Phoebus, 1992; Hogan and Rosmond, 1991; Hogan and Brody, 1993) has a model top of 1 hPa and prior to12UTC September 18 2002 operated with horizontal triangular truncation T159 and 24 model levels but after this date switched to T239 and 30 model levels. The model levels in the current operational system are pure sigma and there are 6 model levels below 850 mb. The analyses and forecasts are output on standard pressure levels of 1000, 975, 950, 925, 900, 850, 700, 500, 400, 300, 250, 200,150, 100, 70, 50, 30, 20, 10 hPa. A 2nd order diffusive term is added to the temperature tendency equation at the top model level, so that the top two levels relax toward an isothermal state. Furthermore, a fourth-order horizontal diffusion operator applied to model vorticity, divergence and temperature is increased by a factor of 5 in the top model level, and by a factor of 2 in the second level from the top. This sponge thus extends over the 1-15 hPa pressure levels.

[1] http://www.bom.gov.au
[2] http://www.ecmwf.int/
[3] https://www.fnmoc.navy.mil/PUBLIC/

Details of the NCEP[4] and UKMO[5] models and analyses can be found at their web sites listed below.

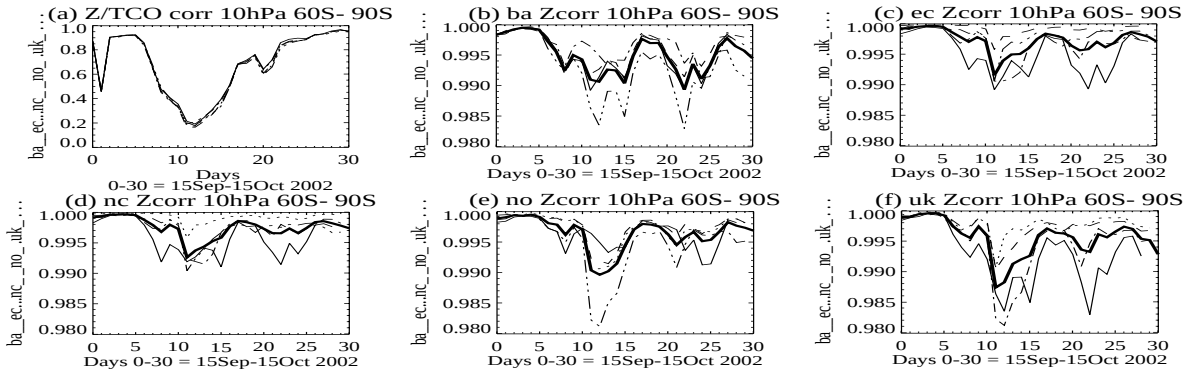

Figure 3: (a) Correlation between daily southern hemisphere TOMS total column ozone (DU) and BAM, ECMWF, NCEP, NOGAPS and UKMO analyses 10 hPa geopotential heights (m). (b)-(f) show correlations between each model BAM, ECMWF, NCEP, NOGAPS and UKMO, respectively, 10 hPa geopotential heights (m) analyses and the other model analyses. All calculations are averaged over latitudes 60^oS *to* 90^oS *and plotted against days from 15 September 2002 to 15 October 2002 (Days 0-30). The thick line in (b)-(f) is the average and the line-styles of the curves are indicated on the plots.*

The NWP centres were asked to provide the following model fields at UTC times 06Z, 12Z, 18Z and 00Z: zonal wind (ms^{-1}), meridional wind (ms^{-1}), geopotential height (m), temperature (K), relative humidity (%) on pressure levels $> 500hPa$, sea level pressure (hPa) and isentropic potential vorticity at 375, 425, 475 and 525 K. These data were requested on a 2.5 x 2.5 latitude/longitude grid and on pressure levels at a vertical resolution that included a significant subset of the following vertical levels - 1000, 850, 500, 200, 100, 70, 50, 30, 10, 7, 5, 3, 1 hPa.

The period of study in each hemisphere for the WGNE study was selected to be when there were large changes in the polar vortex. The northern hemisphere target period was 15 January 2000 - 15 February 2000 (32 days, inclusive) for the analyses and 29 January 2000 - 7 February 2000 (10 days, inclusive) for the forecasts and was selected because of a developing planetary wave three in the lower stratosphere associated with tropospheric blocking, cold temperatures and a developing warming (Newman *et al.* 2002). The southern hemisphere target period was 15 September 2002 - 15 October 2002 (31 days, inclusive) for the analyses and 20 September 2002 - 3 October 2002 (14 days, inclusive) for the forecasts. This period was selected because it was an active period for the polar vortex - the first recorded major sudden warming. This report will only look into the southern hemisphere part of the WGNE study.

2 Southern hemisphere analyses comparison

In order to examine the vortex evolution simulated by the various model analyses we compare model fields with an independent depiction of the vortex evolution, namely the TOMS total column ozone (TCO) field. Total column ozone has been shown to be well correlated with stratospheric geopotential height and temperature (Petzoldt *et al.*, 1994; Vaughan and Price, 1991; Teitelbaum *et al.*, 1998; Newman and Lait, 1988; Ohring and Muench, 1960). This can be understood during quiescent vortex periods, when the vortex is generally symmetric and centred on the pole, because the TCO is an integrated quantity. However during active vortex periods, such as sudden warming events, this correlation would not be expected to be as strong because the

[4]http://www.nco.ncep.noaa.gov/
[5]http://badc.nerc.ac.uk/data/ukmo.html

vortex has a more complicated vertical structure, involving variations in both vortex centre and elongation with height (Waugh 1997).

The evolution of the polar vortex as seen by TOMS TCO on polar stereographic plots from 15 September 2002 to 15 October 2002 (Days 0-30) can be seen in Figure 2 while Figure 3(a) shows the correlation between TOMS TCO and 10 hPa geopotential height fields, averaged for latitudes 60^oS to 90^oS, from all the models. Figure 3(b)-(f) shows the correlation between the BAM, ECMWF, NCEP, NOGAPS and UKMO, respectively, 10hPa geopotential height fields for this period with each of the other model analyses 10hPa geopotential height fields, again all averaged for latitudes 60^oS to 90^oS.

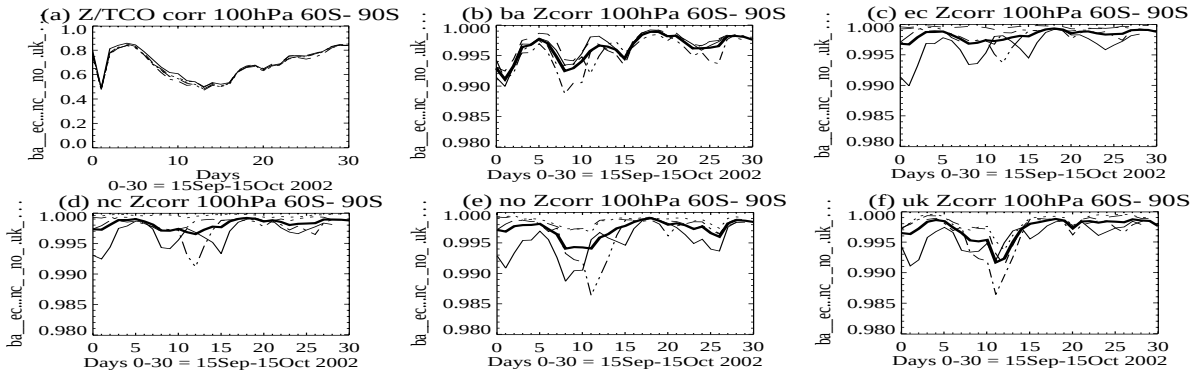

Figure 4: (a) Correlation between daily southern hemisphere TOMS total column ozone (DU) and BAM, ECMWF, NCEP, NOGAPS and UKMO analyses 100 hPa geopotential heights (m). (b)-(f) show correlations between each model BAM, ECMWF, NCEP, NOGAPS and UKMO, respectively, 100 hPa geopotential heights (m) analyses and the other model analyses. All calculations are averaged over latitudes 60^oS *to* 90^oS *and plotted against days from 15 September 2002 to 15 October 2002 (Days 0-30). The thick line in (b)-(f) is the average and the line-styles of the curves are indicated on the plots.*

During this period the polar vortex underwent the first recorded major sudden warming to occur in the southern hemisphere. The polar vortex, whose edge is indicated by the shaded TCO 200-240 DU contour region in Figure 2, is within the $\sim 60^oS$ latitude from the 15 - 17 September (Days 0-2) but by 18 September (Day 3) it elongates along the $\sim 135^oE$ - $\sim 45^oW$ axis with the lobe near $\sim 135^oE$ rotating eastward faster than the $\sim 45^oW$ lobe. This causes the vortex to assume a "jellybean" shape and move off the pole by 21 September (Day 6) with the first sign of a splitting of the vortex occurring on 22 September (Day 7) when two centres of low TCO form near $\sim 60^oS$ at $\sim 0^oE$ and $\sim 115^oW$. These two low TCO centres will be referred to as the El and Wl centres.

These centres elongate, rotate slowly eastward and move equatorward during 23-25 September (Days 8-10).The separation is complete by 26-27 September (Days 11-12) when the western centre Wl has moved to longitude $\sim 90^oW$ and shrunk in size while the eastern centre El is still on the $\sim 60^oS$ latitude but has shifted to $\sim 40^oE$. These two centres then remain relatively stationary, but shrink and elongate, until the 29 September (Day 14) when the western centre Wl has decayed. The remaining El centre drifts eastward and poleward, elongates and grows in size, though never regains the size of the initial vortex, until 3 October (Day 18) when a "jellybean" shape is again formed with elongations along the $\sim 0^oE$ and $\sim 100^oE$ longitudes. The easterly lobe then retracts so the vortex is almost circular and located at $\sim 5^oE$ and $\sim 75^oS$ on 5 October (Day 20). The vortex orientation then rotates rapidly eastward, drifts back to the pole and undergoes elongation to 12 October (Day 27). It then becomes polar centred and symmetric from 13-15 October (Days 28-30). Thus, over this period the vortex goes from a reasonably strong relatively symmetric polar centred vortex through the breakdown and split into two vortex centres, where one decays and the remaining weakened vortex is again

polar centred and symmetric.

The TOMS TCO correlation with 10 hPa geopotential height shown in Figure 3(a) indicates that during this period there is strong correlation ($>$ .9) between TOMS TCO and all the analyses 10 hPa geopotential height fields initially, except for the spike at Day 2 due to loss of TOMS data, but this correlation drops dramatically from Day 5, when the vortex is deformed into a "jellybean" shape prior to splitting, to its lowest value at Day 12, when the split is complete, starts to return and then drops again on Day 19 to a localized minima on Day 20, when again it changes from "jellybean" shape to circular, and then recovers to $>$ .9 values. All the model analyses show almost identical curves in this plot.

The correlation between the model analyses 10 hPa geopotential heights Figure 3(b)-(f) also show reduced correlations starting at Day 5, minimizing at Day 11-12 recovering and then reducing again from Day 17 to have local minima again near Day 21-22 and Day 24. Note that though all these correlations are larger than .98, which we would expect from analyses of the same events, the times when these analyses are least correlated coincide with when the vortex is undergoing its most rapid changes. This implies that even the analysis systems have trouble with the vortex during such rapid changes.

Some of the characteristics of these correlation patterns are mimicked at other vertical levels as can be seen in the corresponding correlation plots for 100 hPa shown in Figure 4. The average and variance of these correlations are both lower at this level than at 10 hPa but Day 5 again shows as the day when all the correlations start to reduce. In Figure 4(a) Days 11-12 are again the days with the lowest TCO correlations and all the model curves are again almost identical. The inter-model correlations in Figure 4(b)-(f) all show a sharp reduction in correlation on Day 5, as at 10 hPa, and the minima again occurs on Days 11-12 for the NCEP and UKMO models but now appears on Day 8 for the BAM, ECMWF and NOGAPS cases.

Figure 5 shows the root mean square error (RMSE) between the model analyses of the geopotential height at 10 hPa and 100 hPa for latitudes 60^oS to 90^oS between all the models. The 10 hPa geopotential height errors

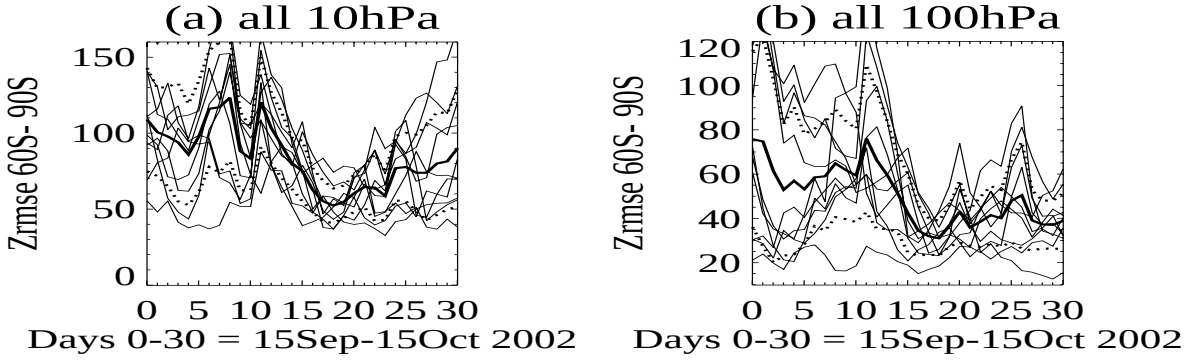

Figure 5: RMSE between daily model analyses geopotential height (m) between all models at (a) 10 hPa and (b) 100 hPa. All calculations are averaged over latitudes 60^oS to 90^oS and plotted against days from 15 September 2002 to 15 October 2002 (Days 0-30). The thick continuous curves are the mean while the thick dotted curves are the mean plus and minus the standard deviation.

rapidly rise from Day 5-8, reduce at Day 9-10, and then there is a peak at Day 11-12, corresponding to the correlation peak above, in all the model analyses. However the correlation peak near Day 20 is only weakly represented in all the analyses, while they all show indications of a peak in RMS error near Day 7, which is the largest error in the BAM and UKMO analyses. In the 100 hPa geopotential height RMSE plots, again the high Day 11-12 error is present in all analyses, though now an error near Day 0 is also strongly represented. Note that there is a steep reduction in the RMSE from Day 10 to Day 15, corresponding to the rapid improvement in TOMS correlations in Figures 3 and 4, and this separates the high error period before this time from the low

error period after this time.

During the maximum TOMS correlation periods (Days 0-5 and Days 22-30) the vortex is a single well defined ellipse as are the corresponding analyses geopotential height fields. But during the poor correlation period (Days 6-21, Figures 3 and 4) the vortex is undergoing rapid changes and all the analyses cannot capture this, though they are all similar to each other. An example of this is seen in Figure 6.

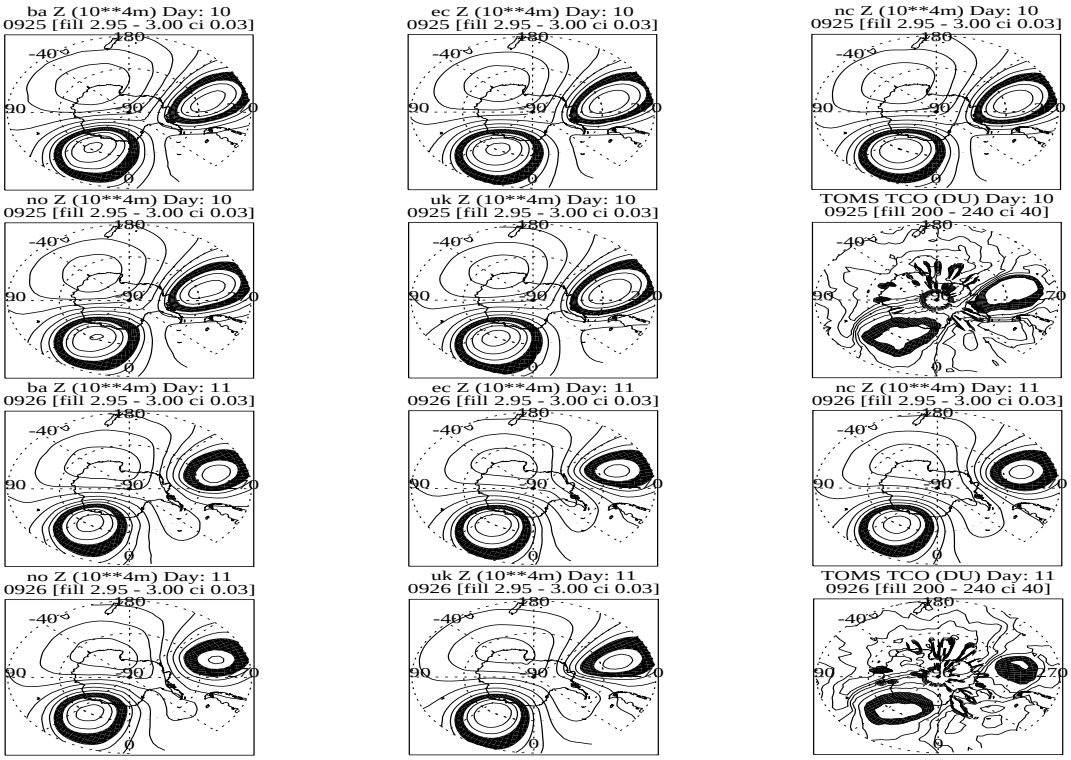

Figure 6: Southern hemisphere polar stereographic plots, for latitudes 40^oS to 90^oS, of the 10 hPa geopotential height field (m) for the BAM, ECMWF, NCEP, NOGAPS and UKMO analyses and TOMS TCO (DU) for (top 8 plots) 25 September (Day 10) and (bottom 8 plots) 26 September (Day 11). The geopotential heights are scaled by 10,000, have a contour interval of 0.03 with shading between 2.95-3.00 10^{4}m. The TCO contour interval is 40 DU, with shading between 200-240 DU. The Greenwich Meridian is at the bottom with the 40^oS and 60^oS latitude circles marked.

This figure shows that all the analyses capture the Wl centre reasonably well showing its large elliptical nature on Day 10 changing to smaller and more equatorward on Day 11, but they all have more circular El centres, which are weaker in the NCEP and NOGAPS cases on Day 10, but by Day 11, ECMWF and UKMO have larger El centres with ECMWF and NCEP having stronger ridging across the pole and UKMO a more elliptical Wl centre. However TOMS shows the El centre as being more elliptical with orientation rotating easterly about its own centre between Day 10 and 11. This misrepresentation of the two centres is the main cause of the decrease in the model analyses and TOMS correlation seen in Figure 3 before Day 12 while the increase in correlation after this time is due to the better representation of the El centre.

Thus, these model analyses are all similar, highly correlated with each other and have small differences in RMSE. The correlation with TOMS TCO is almost identicle for all the models and shows high correlations when the vortex is symmetric and located on the pole but rapidly decreases as the polar vortex undergoes rapid changes. This is seen when the vortex starts to split on Day 5 and has its minimum on Days 11-12 when the Wl centre rapidly decays. This period, Days 11-12, is also when a steep improvement in RMSE is found at 10

and 100 hPa levels.

3 Southern hemisphere forecast comparison

If a NWP model has problems with forecasting a particular day this could be due to a variety of errors with the two main ones being initialization problems or difficulties with a particular dynamic situation in the atmosphere. If the problem is the former, then we would expect the error to occur on the given initialization day but not necessarily on future days whereas if the problem is the latter then we may expect the error to propagate with the difficult forecast day as we progress through future forecasts.

In order to examine this proposition, we plot in Figure 7 the 30 hPa temperature RMSE between the model forecasts and their respective analyses starting at 00UTC on 20 September (Day 5) for 14 days to 12UTC 3 October 2002 (Days 18.5) averaged over latitudes 60^oS to 90^oS for the four models we have forecasts for ie BAM, ECMWF, NCEP and NOGAPS. Note that as seen in Table 1, these models have forecasts out to 8, 10, 10 and 5 days, respectively. The average of these RMSE values over the initialization and forecast days can be seen in Figure 8.

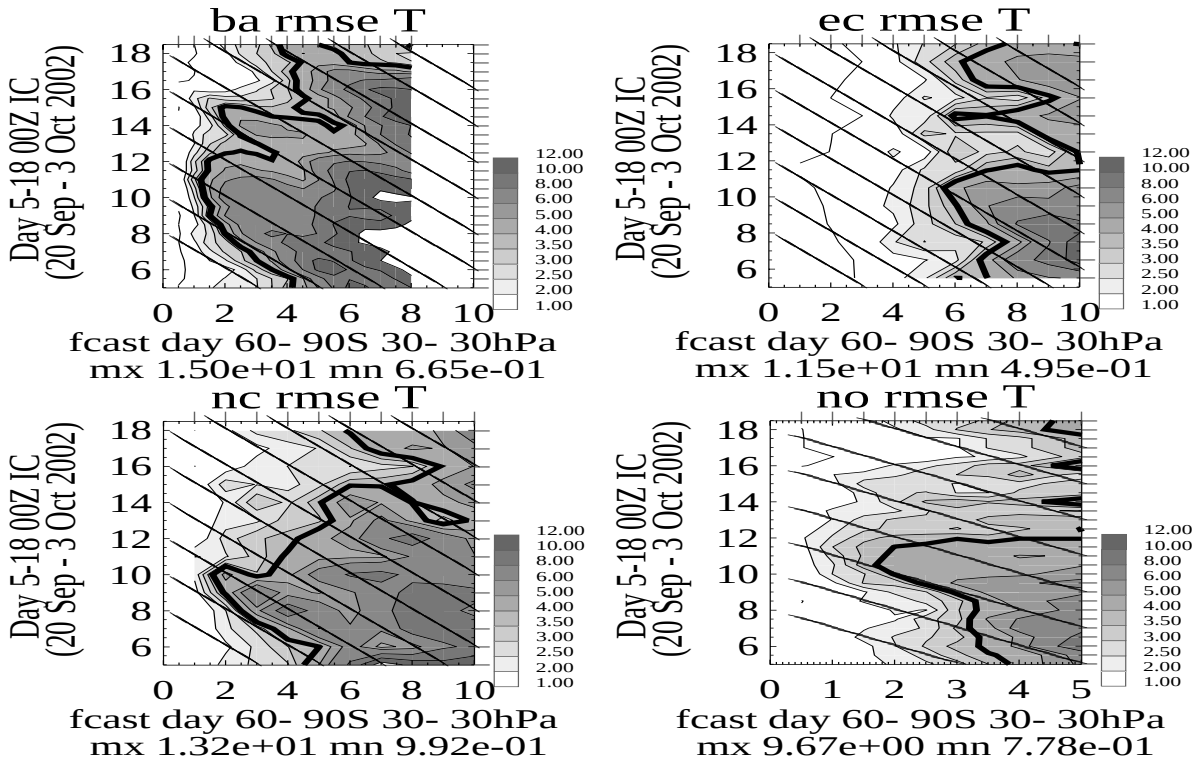

Figure 7: Plots of forecast day (0-10) against initialization analysis day from 00UTC 20 September to 12UTC 3 October 2002 (Days 5-18.5) of the 30 hPa temperature field (K) RMSE between the BAM, ECMWF, NCEP and NOGAPS forecasts and their respective analyses averaged over latitudes 60^oS *to* 90^oS*. The maximum and minimum is below each plot, the diagonals are lines of constant verification day, NOGAPS only goes out to 5 days and contour intervals are the same and are indicated. The thick contour is the* 4*K contour line.*

These contour plots show that while all the model forecast errors generally grow with forecast day, there is also strong day-to-day variation present in these errors. The left plot in Figure8 shows this increasing error clearly and the fact that the BAM model has the fastest growing error followed by NOGAPS and NCEP, which are very

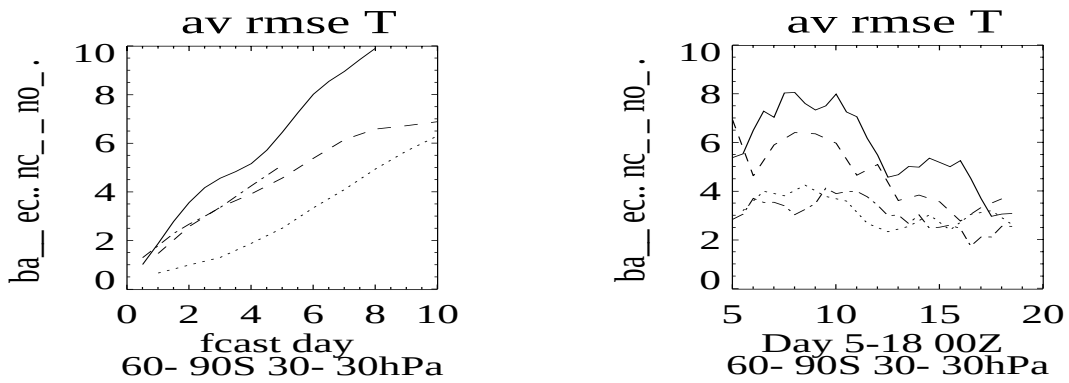

Figure 8: Plots of the mean 30 hPa BAM, ECMWF, NCEP and NOGAPS temperature fields (K) RMSE taken from Figure 7 and (left) averaged over initiation day for forecast days (0-10) and (right) averaged over forecast day for initiation Days 5-18.5. The line style for each model is indicated.

similar, while ECMWF has the slowest growing error but its gradient after forecast day four is essentially the same as NOGAPS and NCEP while NCEP also has a steadying of the average RMSE after eight days. Thus BAM generally has the largest errors while ECMWF has the least, indeed BAM has the largest maximum RMSE and ECMWF the lowest maxima, even though ECMWF has forecasts out to ten days and NOGAPS only out to five. The variability in the RMSE can be seen by considering the 4*K* contour line in Figure7 which varies between: 1.5-8 days for BAM and NCEP; 6-10 days for ECMWF; and, 2-5 days for NOGAPS.

Figure 7 shows that for forecasts initiated on Days 5-10 (20-25 September) all the models have almost continuously increasing RMSE for any given forecast. This implies that over this period there is a steady reduction of forecast skill and that this is an increasingly difficult period for all the models. Figure2 shows that this period is when the vortex is splitting in two and the previous section also shows that this period is when the TCO/analyses and inter-analyses correlations dropped rapidly. From initialization Days 10-12 (25-27 September) the skill in all the models is seen to improve, though this is not as clear in the NOGAPS contour plot - probably due to their forecasts only going out to five days, and this is addressed below. This can be seen more clearly in the right plot of Figure 8 where all the models show that initialization Days 10-12 (25-27 September) separate an initial large error period from a relatively smaller error period. The previous section showed that this period also performed a similar function for the inter-analyses RMSE and the TCO/analyses and inter-analyses correlations had their lowest values.

Are similar characteristics seen in shorter range forecasts? To determine this we re-create Figure7 but only for forecasts out to five days. The results can be seen in Figure9. The same characteristics, though more clear, are seen as for Figure 7 but now all the models show a steady reduction in skill over initialization Days 5-10 and an increase in skill after initialization Days 10-12.

Can these RMSE difficulties be related to particular days? If this is true then there should be a strong dependence of the RMSE on the verification day, where lines of constant verification day are indicated by the diagonals in Figures 7 and Figure 9. In both figures there are contoured regions which extend along the verification diagonals encompassing one or several verification days. In the ten-day forecast plots (Figure7) the BAM model has such extensions around verification Days 10-14, 16-17 and 20-22 while: NCEP has extensions centred on Days 12 and 17; NOGAPS has extensions centred on Days 12-14 and 17; while ECMWF has no such clearly defined extensions. The five-day forecasts (Figure9) show these extensions more clearly and now extensions can also be seen in the ECMWF model on Days 12-13 and 17-18. Thus all the models show that the periods 27-28 September (Days 12-13) and around 2 October (Day 17) are dynamical situations which they have difficulty with forecasting. These periods are when the westerly vortex (Wl) is decaying and when

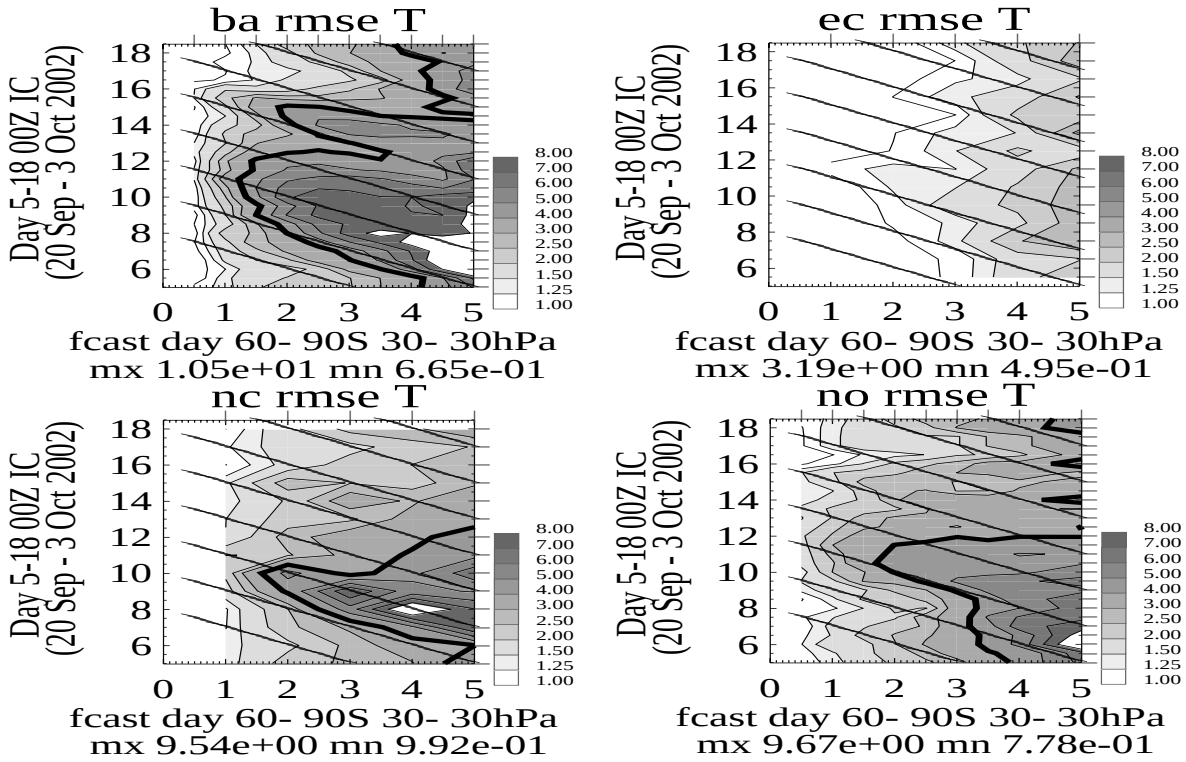

Figure 9: As in Figure 7 but only for forecasts out to five days.

the easterly vortex (El) is moving westward (Figure 2).

These characteristics are also seen in corresponding plots for other fields. Figure 10 shows RMSE contour plots corresponding to Figure 7 but for the geopotential height, zonal wind, temperature and meridional wind fields for the BAM model. Again, initialization Day 12 separates the difficult/easier forecasting periods and strong verification day dependence is seen on Days 10-14, 16-17 and 20-22 for all the fields.

How do these plots look at other vertical levels? To demonstrate this we show RMSE plots corresponding to Figure 7 but for the BAM temperature field at 10, 50, 110 and 200 hPa pressure levels in Figure 11. As in Figure 7 all the plots show a steady decrease in skill over initialization Days 5-10 and a sudden increase in skill after initialization Day 12. However while levels above 50 hPa show that this error remains small, levels at and below 50 hPa have this error growing quickly to values similar to pre-Day 12 levels. Thus Day 12 has lower errors on all the vertical levels but the increase in skill after this day decreases as we progress deeper into the atmosphere ie there is less variability in the errors. The strong verification day dependence seen at 30 hPa in Figure 7 can be seen in levels at and above 50 hPa, with it being strongest at 10 hPa. However below 50 hPa the error contours are more parallel to the horizontal axis and are thus more dependent on the initialization day. This becomes more pronounced as we progress further down into the atmosphere where there is more horizontal spiking eg initialization Day 8.5 at 200 hPa. However, Day 11 can still be seen as diagonally dependent even down to 200 hPa. The forecasts also have smaller error magnitudes the lower we get.

Plots of the RMSE on pressure versus forecast days show the progression of the verification day errors through time. An example of this can be seen in Figure 12 where plots for the twelve hourly BAM forecasts from 00UTC 20 September to 00UTC 27 September (Days 5-12) depict contours of normalized RMSE on forecast day against pressure level (from 100-10 hPa) axes.

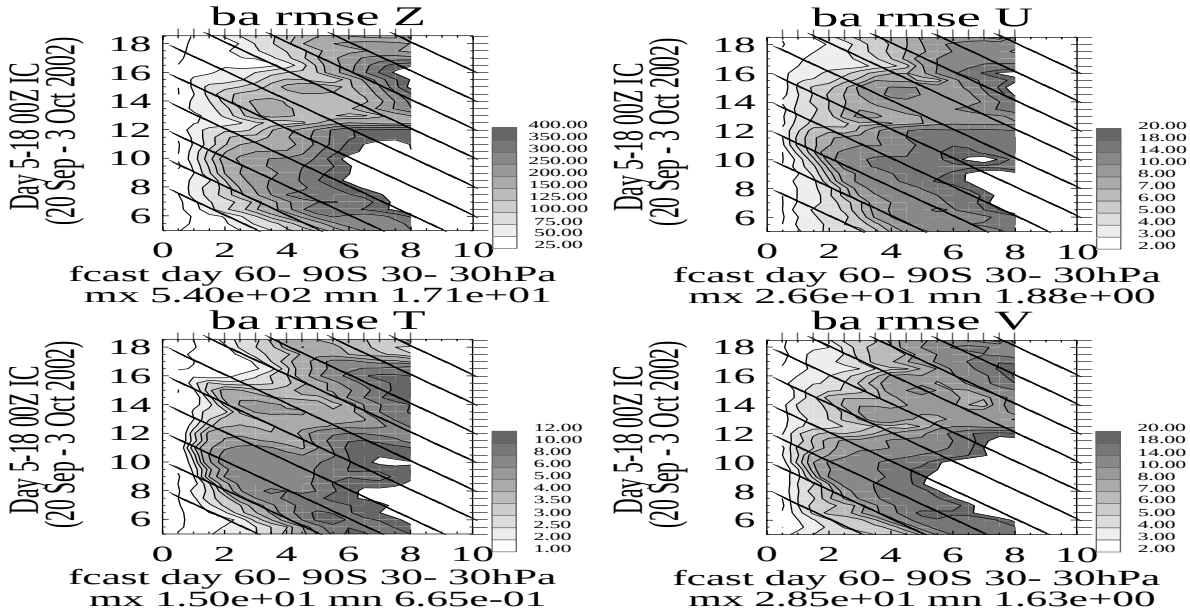

Figure 10: Plots of forecast day (0-10) against initialization analysis day from 00UTC 20 September to 12UTC 3 October 2002 (Days 5-18.5) of the 30 hPa geopotential height (m) , zonal wind (ms^{-1}), temperature (K) and meridional wind (ms^{-1}) field RMSE between the BAM forecasts and their respective analyses averaged over latitudes 60^oS *to* 90^oS*. The maximum and minimum is below each plot, the diagonals are lines of constant verification day and contour intervals are indicated.*

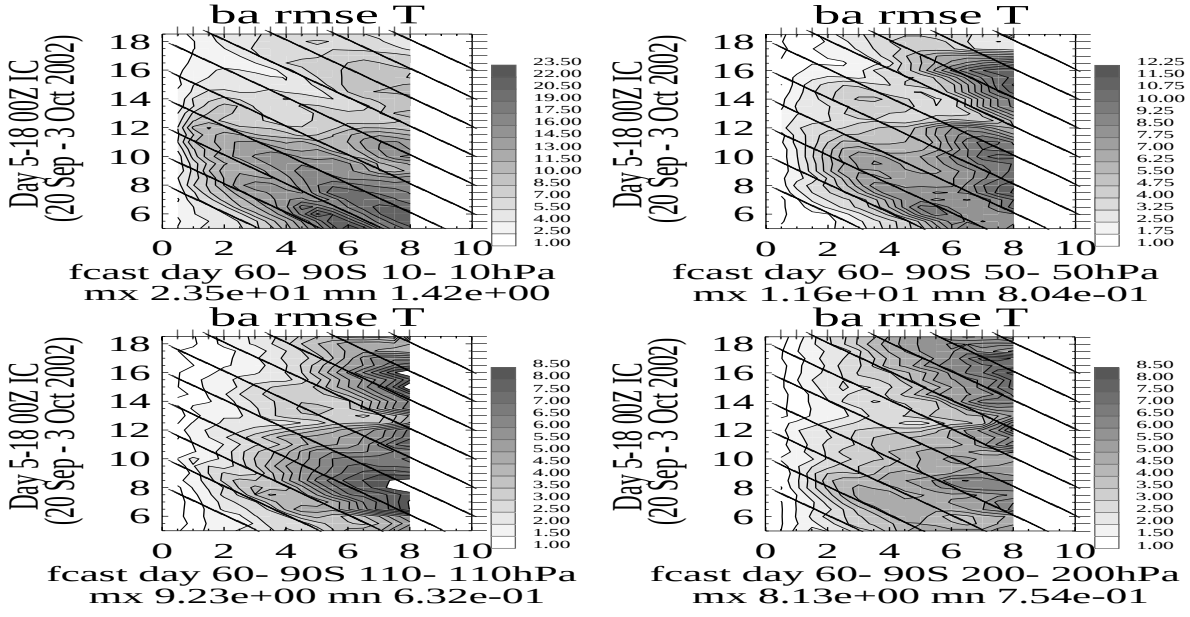

Figure 11: Plots of forecast day (0-10) against initialization analysis day from 00UTC 20 September to 12UTC 3 October 2002 (Days 5-18.5) of the 10, 50, 110 and 200 hPa temperature (K) field RMSE between the BAM forecasts and their respective analyses averaged over latitudes 60^oS *to* 90^oS*. The maximum and minimum is below each plot, the diagonals are lines of constant verification day and contour intervals are indicated.*

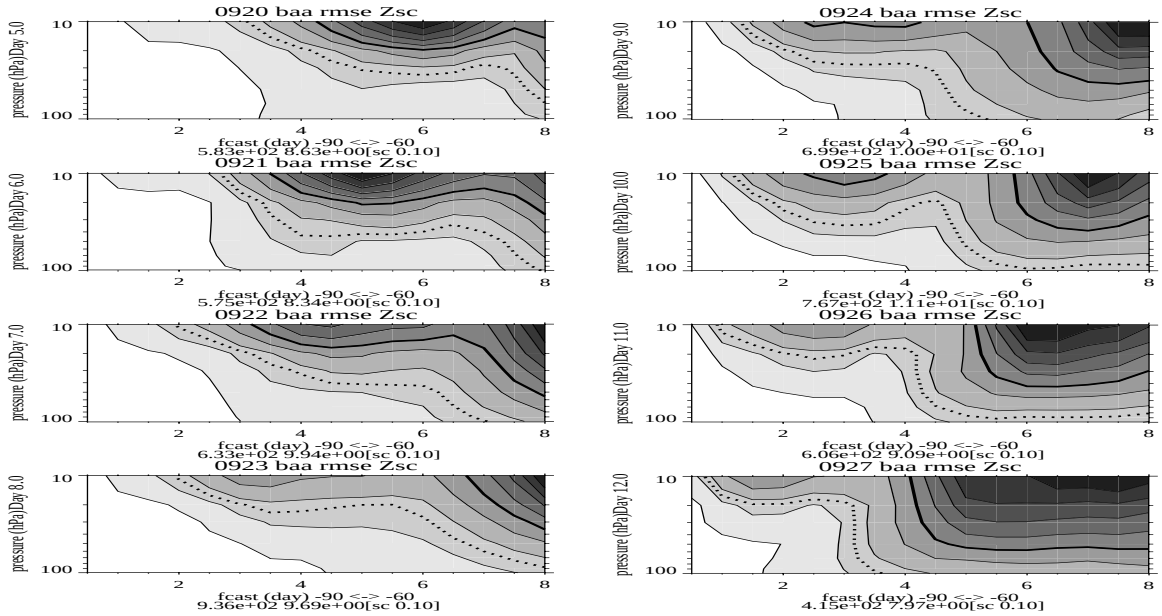

Figure 12: Normalized RMSE geopotential height forecast day vs log pressure (100-10 hPa) contour plots for BAM twelve hourly forecasts for initialization days 20 September to 27 September, at 00UTC, (Days 5-12) averaged over the latitude range 60^oS *to* 90^oS*. The contour interval is* 0.1 *from* $0.1 - 0.9$ *with the shading progressing from light to dark, thick dotted and continuous lines are the* .25 *and* .5 *contours and the maximum and minimum non-normalized RMSE values are below each plot.*

The first thing to note about this figure is that the normalized error descends from 10 hPa for increasing forecast days and that this seems to go in steps. Thus in the 20 September (Day 5) initialized plot the .25 normalized RMSE contour drops on forecast day 3 from 10 hPa to 30 hPa by forecast day 5, remains there until forecast day 7 and then drops down to 100 hPa. This stepping is common to all the plots, but does not occur on the same forecast days. The maximum error always appears at the top but is not always for the most extreme forecast, forecast day 8. Rather these maxima are seen to be associated with the steps in error. The first error maxima at 10 hPa can be seen on the plots for initialization Days 5-12 to occur on forecast days 6, 5, 4.5, 3.5, 2.5-4, 3, 2.5 and 1.5, respectively, which correspond to verification Days 11, 11, 11.5, 11.5, 11.5-13, 13, 13.5 and 13.5, respectively. Thus there are normalized RMSE errors at 10 hPa, which also extend down to ~ 30 hPa, associated with verification Days ~ 11.5 and ~ 13.5, which can also be clearly seen in the BAM RMSE temperature contours at 10 hPa in Figure 11.

A second 10 hPa level error maxima, which has a larger vertical extent than the first and corresponds to the second "step" mentioned above, can be seen to move from forecast day 8 in the initialization Days 9-12 plots and to occur on forecast days 7.5-8, 7, 6-6.5 and 5-8, respectively, corresponding to verification Days 16.5-17, 17, 17-17.5 and 17-20, respectively. This second 10 hPa maxima, which extends down below ~ 100 hPa, is thus associated with verification Day ~ 17.5 and can again be seen in Figure 11. Thus this figure shows that verification Days ~ 11.5, ~ 13.5 and ~ 17.5 are dynamic situations which the BAM model has more difficulty with that other days for this study.

The descent deeper into the atmosphere of the normalized RMSE errors can be explained by model top error, BAM had a model top at 10 hPa for these runs, associated with the damping mechanisms often applied near the model top, progressing down and contaminating the lower levels as the forecasts are extended. That these errors are associated with the model top can be demonstrated by recreating this plot but for the ECMWF data, which has data up to 1 hPa and a model top at 0.1 hPa, for 20 September to 3 October in Figure 13 . The

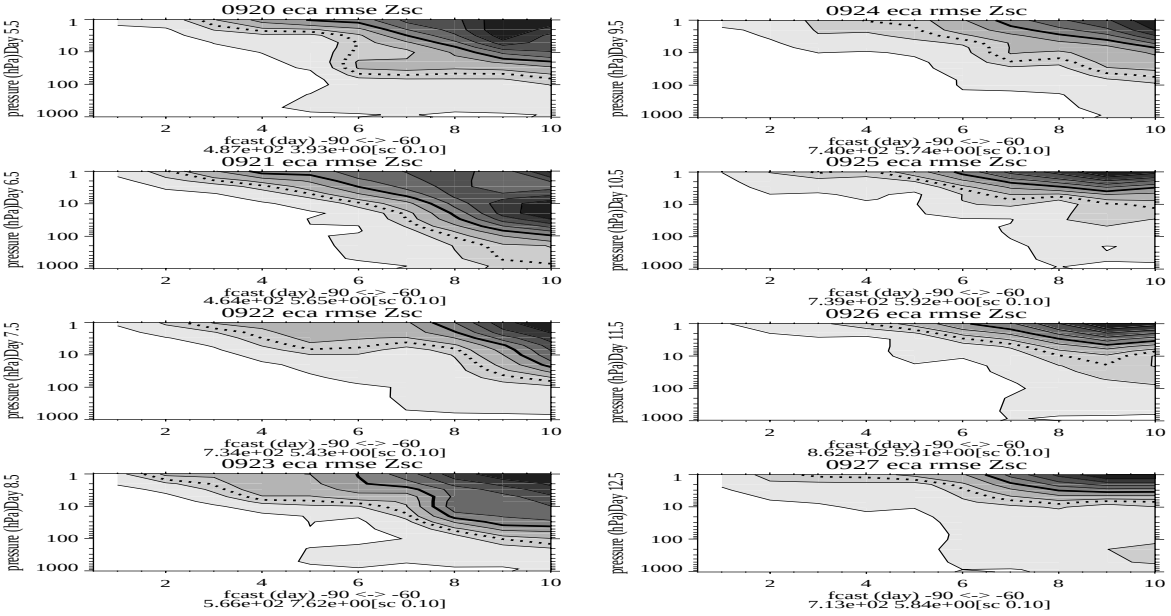

Figure 13: Normalized RMSE geopotential height forecast day vs log pressure (1000-1 hPa) contour plots for ECMWF twenty-four hourly forecasts for initialization days 20 September to 27 September, at 12UTC, (Days 5.5-12.5) averaged over the latitude range 60^oS *to* 90^oS*. The contour interval is* 0.1 *from* $0.1 - 0.9$ *with the shading progressing from light to dark, thick dotted and continuous lines are the* .25 *and* .5 *contours and the maximum and minimum non-normalized RMSE values are below each plot.*

maximum errors are again seen to be associated with the model top and extend down, in a step-wise manner, to the lower levels as the forecasts are extended in time for any given initialization day. Note also that there is often better skill, smaller normalized RMSE error, at 50-100 hPa than at 300-500 hPa. This observation is also seen in similar plots for the geopotential height, zonal wind, temperature and meridional wind fields from all the forecast models used in this paper and has been made in other studies (Waugh *et al.* , 1998; Lahoz, 1999) and can be explained by the stratosphere being dominated by low wave number flows while the troposphere is dominated by high wave number synoptic scale flows.

To see what these forecast errors look like we can create polar stereographic plots of the 30 hPa BAM twelve hourly forecasts (contour lines), overlaying the corresponding verification analyses (filled contours), for forecasts out to six days for initialization day 12UTC 23 September (Day 8.5) in Figure 14. The forecast after 12 hours (verification Day 9.0) shows the forecast contour lines and verification filled contours almost overlapping. The low geopotential height centres associated with the split vortex centres are not as deep in the forecasts at 24 hours (Day 9.5), and this trend continues. The 60 hour forecast (Day 11) has vortices that are starting to be displaced more westward of the analysed vortices. By 72 hours (Day 11.5) the forecast vortices are seen to be more circular than the more elliptical analyses vortices. By 96 hours (Day 12.5) the beginning of a poleward displacement and more easterly orientation of the forecast vortex is seen. By the 144 hour forecast (Day 14.5), the forecast vortex is seen to be: smaller; displaced westward; displaced poleward; have a faster easterly rotation of its orientation and to be more circular.

Are these characteristics of the forecast model similar at other levels? To examine this we construct in Figure 15 plots similar to Figure 14 but for the ECMWF model at 5 hPa. The forecast after 24 hours (verification Day 9.5) shows the forecast contour lines and verification filled contours almost overlapping. The 72 hour forecast (Day 11.5) shows a westward displacement beginning as well as a shrinking of the vortex while the 120 hour forecast (Day 13.5) shows movement of the vortex towards the pole. The final 240 hour forecast (Day

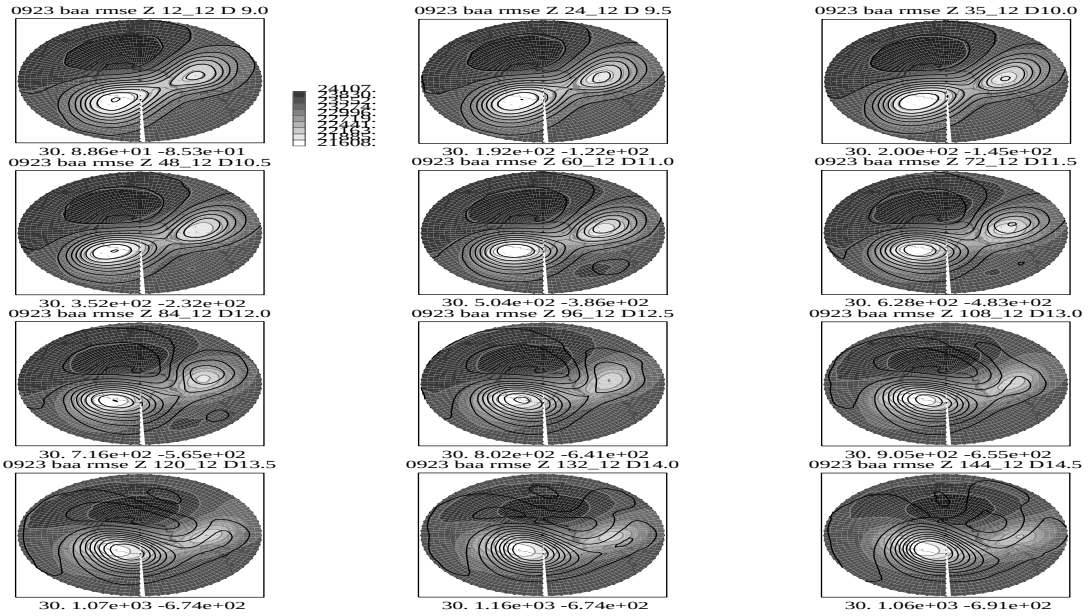

Figure 14: 30 hPa polar stereographic plots of the geopotential height (m) field for the BAM twelve hourly forecasts initiated at 12UTC on 23 September (Day 8.5) and plotted out to forecast day six, which corresponds to verification Days 9-14.5. The forecasts are the line contours while the corresponding analyses are the filled contours. The forecast time (in hours) and corresponding verification Day (eg D 9.0 in the first plot) are at the top of each diagram.

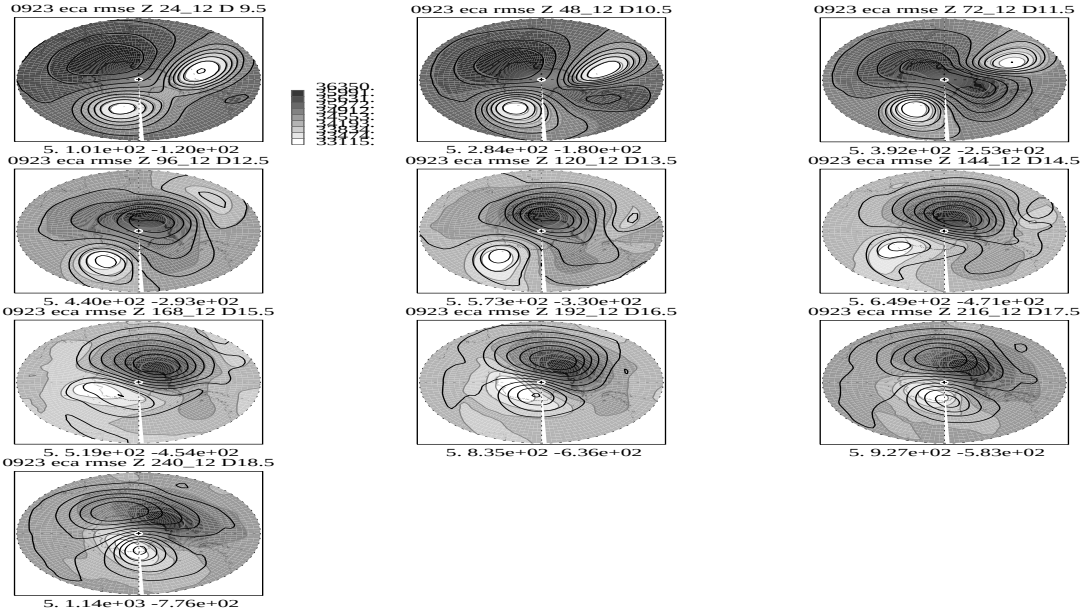

Figure 15: 5 hPa polar stereographic plots of the geopotential height (m) field for the ECMWF twenty-four hourly forecasts initiated at 12UTC on 23 September (Day 8.5) and plotted out to forecast day ten, which corresponds to verification Days 9.5-18.5. The forecasts are the line contours while the corresponding analyses are the filled contours. The forecast time (in hours) and corresponding verification Day (eg D 9.5 in the first plot) are at the top of each diagram.

18.5) shows all the characteristics displayed in Figure 14 ie a forecast vortex which is smaller, more circular, more poleward and more eastwardly displaced and with a more easterly orientation, though the latter is not as obvious as in the BAM case seen in Figure 14.

These differences between the forecast vortex and the analysed vortex are seen in all the models for levels at and above 100 hPa eg we plot in Figure 16 the 50 hPa polar stereo plot of the geopotential height field for the first and last forecast from each of the models initiated on 23 September. We can see the large changes that the

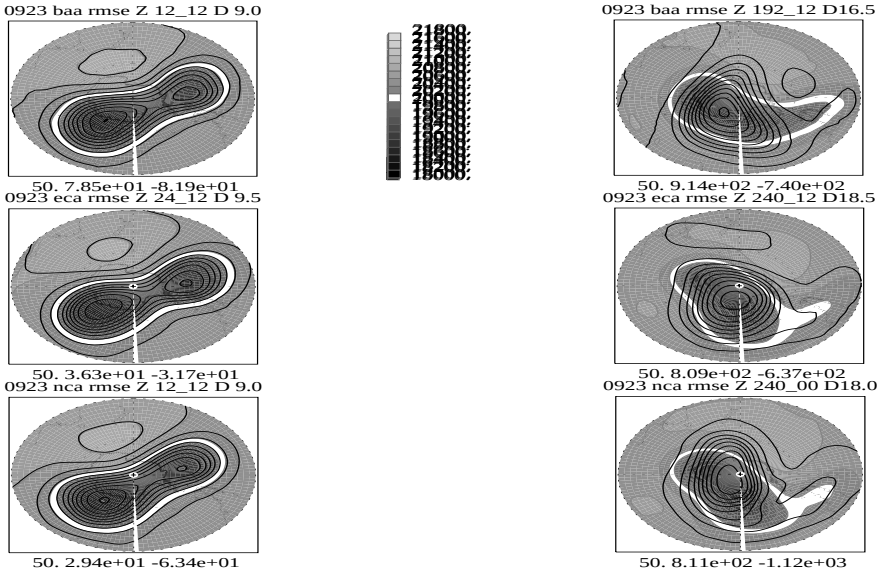

Figure 16: 50 hPa polar stereo plot of the geopotential height (m) field for the (left) first and (right) last forecast from each of the models (top) BAM, (middle) ECMWF and (bottom) NCEP initiated on 23 September.The forecasts are the line contours while the corresponding analyses are the filled contours. The forecast time (in hours) and corresponding verification Day (eg D 9.0 in the first plot) are at the top of each diagram.

vortex undergoes over this period, going from a two cell vortex to a single cell, but all the models show a final forecast vortex which is smaller, more circular, more poleward and more westerly displaced and with a more easterly orientation, though the latter is not as obvious in the ECMWF case. The creation of a smaller, more circular and more polewardly displaced vortex indicates that all the models are trying to create weaker and less disturbed vortices. Similar forecast anomalies have been reported by Waugh *et al.* (1998) and Lahoz (1999).

4 Summary

We have examined the stratospheric analyses and forecasting ability of five NWP models (BAM, ECMWF, NCEP, NOGAPS and UKMO) during the southern hemisphere major sudden warming of 2002.

All the BAM, ECMWF, NCEP, NOGAPS and UKMO NWP analyses 10 hPa geopotential heights have almost identical correlations with TOMS TCO which are very high when the polar vortex is quiescent. However when the vortex undergoes rapid changes these correlations reduce drastically until the vortex is again quiescent. This can be understood because the TCO is an integrated quantity and during quiescent vortex periods the vortex is generally symmetric and centred on the pole but during active vortex periods, such as the sudden warming event studied in this paper, the vortex has a more complicated vertical structure, involving variations in both vortex centre and elongation with height (Waugh 1997). The reductions in correlation start when the vortex

begins to split and reach their minimum on 26-27 September (Days 11-12) when the western centre of the split vortex begins to rapidly decay. The correlations between the model 10 hPa geopotential height analyses also show a steep reduction 26-27 September (Days 11-12) from their very high values. This period is also a time when the 10 hPa geopotential height RMSE between all the models undergoes a rapid reduction. All of these characteristics are seen at 100 hPa, though not as dramatically.

All the BAM, ECMWF, NCEP and NOGAPS NWP forecasts show that forecasts in this study initialized before 25-28 September (Days 10-13) have skill that is decreasing with initialization date but this skill improves dramatically after this time. This improvement in skill is seen in the geopotential height, zonal wind, temperature and meridional wind fields for all levels at and above 50 hPa. Each of these models shows certain days which are harder to forecast than others eg for the BAM twelve hourly forecasts these days are 12UTC on 26, 28 September and 2 October (Days ~ 11.5, ~ 13.5 and ~ 17.5). All of the models had difficulties with forecasting near these verification days.

The normalized RMSE forecast error associated with all the models has maxima near the model top which propagates down with forecast day, often in a step-wise manner. These steps are generally associated with error maxima near the model top which are often linked to a given verification day and can be seen to propagate with that verification day.

All the model forecasts displayed similar errors in their prediction of the polar vortex evolution. These characteristic errors were that the forecast vortex was seen to be: smaller; displaced westward; displaced poleward; have a faster easterly rotation of its orientation and to be more circular. The creation of a smaller, more circular and more polewardly displaced vortex, characteristics also reported by Waugh *et al.* (1998) and Lahoz (1999), indicates that all the models are trying to create weaker and less disturbed vortices. The westward displacement of the forecast vortex may be due to the damping often applied in the upper levels of NWP models interfering with the vortex flow.

Acknowledgements

I would like to thank: Agathe Untch (ECMWF), Mark Iredell (NCEP), John McCormack (NRL) and Adam Scaife (UKMO) for providing model output; Kamal Puri (WGNE, BMRC) for encouraging this study and Martin Miller (ECMWF) for inviting me to the workshop.

References

Andrews, D. G. (1985). Wave-mean-flow interaction in the middle atmosphere, *Adv. in Geophys.*, **28**, 249–275.

Andrews, D. G., Holton, J. R. and Leovy, C. B. (1987). Middle Atmosphere Dynamics, *International Geophysics Series*, **40**, Academic Press, pp489.

Atkinson, R., Grainger, S. and Udelhofen, P. M. (1997). A scheme for the routine analysis and deterministic prediction of the global total ozone distribution. In *Proceedings of AMS International Conference on the Meteorology of the Southern Hemisphere, Pretoria, Africa*.

Baldwin, M. P. and Dunkerton, T. J. (1999). Propagation of the Arctic Oscillation from the stratosphere to the troposphere. *J. Geophys. Res.*, **104**, D22, 30,937–30,946.

Baldwin, M. P. and Dunkerton, T. J. (2001). Stratospheric harbingers of anomalous weather regimes. *Science*, **294**, 581–584.

Baldwin, M., Horooka, T., O'Neill, A. and Yoden, S. (2003). Major stratospheric warming in the southern hemisphere in 2002: Dynamical aspects of the ozone hole split, *SPARC Newsletter*, **20**, 24–26.

Bayler, G. and H. Lewit (1992). The Navy Operational Global and Regional Atmospheric Prediction System at the Fleet Numerical Oceanography Center", *Weather and Forecasting*, **Vol. 7**, 2, 273–279.

Bourke, W. P. (1974). A multi-level spectral model I: Formulation and hemispheric integrations. *Mon. Wea. Rev.*, **102**, 687–701.

Bourke, W. P., McAvaney, B., Puri, K., and Thurling, R. (1977). Global modelling of atmospheric flow by spectral methods. *Methods in Computational Physics*, **17**, Ed. J. Chang, Academic Press, New York, 267–324.

Bourke, W. P. (1988). Spectral methods in climate models. *Physically-Based Modelling and Simulation of Climate and Climatic Change, Part 1*, Ed. M.E. Schlesinger, Kluwer Academic Publishers, Dordrecht, 375–431.

Bourke, W., Hart, T., Steinle, P., Seaman, R., Embery, G., Naughton, M. and Rikus, L. (1995). Evolution of the Bureau of Meteorology's global data assimilation and prediction system. Part 2, *Aust. Meteorol. Mag*, **44**, 19–40.

Carver, G. D., Norton, W. A. and Pyle, J. A. (1994). A case study in forecasting the stratospheric vortex during EASOE, *Geophys. Res. Lett.*, **21**, 1451–1454.

Colman, R. A., and McAvaney, B. J. (1991). Experiments using the BMRC general circulation model with a heat balance ocean, *BMRC Research Report No. 24*, Bureau of Meteorology Research Centre, Melbourne, Australia, 31 pp.

Goerss, J., and Phoebus, P. (1992). The Navy's operational atmospheric analysis. *Wea. Forecasting*, **7**, 232–249.

Hart, T. L., Gay, M. J., and Bourke, W, (1988). Sensitivity studies with the physical parameterizations in the BMRC global atmospheric spectral model, *Austral. Meteor. Mag.*, **36**, 47–60.

Hart, T. L., Bourke, W., McAvaney, B. J., and Forgan, B. W., (1990). Atmospheric general circulation simulations with the BMRC global spectral model: The impact of revised physical parameterizations. *J. Climate*, **3**, 436–459.

Hartley, D. E., Villarin, J., Black, R. X. and Davis, C. A. (1998). A new perspective on the dynamical link between the stratosphere and troposphere, *Nature*, **391**, 471–474.

Hartmann, D. L., Wallace, J. M., Limpasuvan, V., Thompson, D. W. J. and Holton, J. R. (2000). Can ozone depletion and greenhouse warming interact to produce rapid climate change?, *Proc. Natl. Acad. Sci.*, **97**, 1412–1417.

Haynes, P. H., McIntyre, M. E., Shepard, T. G., Marks, C. J. and Shine, K. P. (1991). On the "Downward Control" of Extratropical Diabatic Circulations by Eddy-Induced Mean Zonal Forces, *J. Atmos. Sci.*, **48**, 4, 651–678.

Hogan, T. F., and Rosmond, T. E. (1991). The description of the Navy Global Operational Atmospheric Prediction System's spectral forecast model, *Mon. Wea. Rev.*, **119**, 1786–1815.

Hogan, T. and Brody L. (1993). Sensitivity Studies of the Navy's Global Forecast Model Parameterizations and Evaluation of Improvements to NOGAPS, *Mon. Wea. Rev.*, **121**, 8, 2373–2395.

Karoly, D. J., Mullenmeister, P. and Bourke, W. (1993). Modelling the spring breakdown of the SH stratospheric vortex. Pp. 149–150 in *Proceedings of the fourth international conference on southern hemisphere meteorology*, 29 March - 2 April 1993, Hobart, Australia. American Meteorological Society, Boston, USA.

Klinker, E. (1994). Diagnosis of the performance of the ECMWF forecasting system in the stratosphere. Pp. 121–146 in the *Proceedings of ECMWF workshop on Stratosphere and numerical weather prediction*, 15–17 November, 1993. European Centre for Medium-Range Weather Forecasts, Reading, UK.

Labitzke, K. (1982). On the interannual variability of the middle stratosphere during the northern winters, *J. Meteorol. Soc. Jpn*, **60**, 124–139.

Lahoz, W. A. (1999). Predictive skill of the UKMO Unified Model in the lower stratosphere. *Q. J. R. Meteorol. Soc.*, **125,** 2205–2238.

Matsuno, T. (1971). A dynamical model of the stratospheric sudden warming, *J. Atmos. Sci.*, **28**, 1479–1494.

McAvaney, B. J., Bourke, W. and Puri, K. (1978). A global spectral model for simulation of the general circulation, *J. Atmos. Sci.*, **35**, 1557-1583.

McAvaney, B. J., Fraser, J. R., Hart, T. L., Rikus, L. J.. Bourke, W. P., Naughton, M. J. and Mullenmeister, P. (1991). Circulation statistics from a non-diurnal seasonal simulation with the BMRC atmospheric GCM: R21L9, *BMRC Research Report No. 29*, Bureau of Meteorology Research Centre, Melbourne, Australia, 231 pp.

McIntyre, M. E. (1982). How well do we understand the dynamics of sudden warmings? *J. Meteorol. Soc. Jpn*, **60**, 37–65.

Mechoso, C. R., Yamazaki, K., Kitcoh, A. and Arakawa, A. (1985). Numerical forecasts of stratospheric warming events during the winter of 1979, *Mon. Wea. Rev.*, **113**, 1015–1029.

Miyakoda, K., Strickler, R. F. and Hembree, G. D. (1970). Numerical simulations of the breakdown of a polar-night vortex in the stratosphere, *J. Atmos. Sci.*, **27**, 139–154.

Newman, P. A., Lait, L. R. and Schoeberl, M. R. (1988). The morphology and meteorology of southern hemisphere spring total ozone mini-holes, *Geophys. Res. Lett.*, **15, 8,** 923–926.

Newman, P. A., Harris, N. R. P, Adriani, A., Amanatidis, G. T., Anderson, J. G., Braathen, G. O., Brune, W. H., Carslaw, K. S., Craig, M. S., DeCola, P. L., Guirlet, M., Hipskind, R. S., Kurylo, M. J., Kullmann, H., Larsen, N., Megie, G. J., Pommereau, J-P., Poole, L. R., Schoeberl, M. R., Stroh, F., Toon, O. B., Trepte, C. R. and van Roozendael, M. (2002). An overview of the SOLVE/THESEO 2000 campaign, *j. Geophys. Res.*, **107**, D20, 10.1029/2001JD001303.

Ohring, G. and Muench, H. S. (1960). Relationships between ozone and meteorological parameters in the lower stratosphere, *J. of Meteo.*, **17,**, 195–206.

Pawson, S. and Kubitz, T. (1996). Climatology of planetary waves in the northern stratosphere, *J. Geophys. Res.*, **101**, D12, 16987–16996.

Petzoldt, K., Naujokat, B. and Neugebohren, K. (1994). Correlation between stratospheric temperature, total ozone, and tropospheric weather systems, *Geophys. Res. Lett.*, **21, 13,** 1203–1206.

Rikus, L. (1991). The role of clouds in global climate modelling. *BMRC Report No. 25*, Bureau of Meteorology Research Centre, Melbourne, Australia, 37 pp.

Shindell, D. T., Schmidt, G. A., Miller, R. L. and Rind, D. (2001). Northern hemisphere winter climate response to greenhouse gas, ozone, solar, and volcanic forcing, *J. Geophys. Res.*, **106**, 7193–7210.

Simmons, A. and Strufing, R. (1983). Numerical forecasts of stratospheric warming events using a model with a hybrid vertical coordinate, *Q. J. R. Meteorol. Soc.*, **109**, 81–111.

Simmons, A. (1994). Some stratospheric aspects of model development at ECMWF. Pp. 23–60 in the *Pro-*

ceedings of ECMWF workshop on Stratosphere and numerical weather prediction, 15–17 November, 1993. European Centre for Medium-Range Weather Forecasts, Reading, UK.

Simmons, A., Mariano, H., Untch, A. and Uppala, S. (2003). Breakdown of the stratospheric winter polar vortex, *ECMWF Newsletter*, **96**, 2–9.

Teitelbaum, H., Moustaoui, M., Van Velthoven, P. F. J., and Kelder, H. (1998). Decrease of total ozone at low latitudes in the southern hemisphere by a combination of linear and nonlinear processes, *Q. J. R. Meteorol. Soc.*, **124,** 2625–2644.

Thompson, D. W. J., Baldwin, M. P. and Wallace, J. M. (2002). Stratospheric connection to northern hemisphere wintertime weather: Implications for prediction, *J. Climate*, **15**, 1421–1427.

Tsuyuki, T. (1994). Impacts if increased vertical resolution in the stratosphere on dynamical extended-range forecasts, *J. Meteorol. Soc. Jpn*, **72**, 6, 795–810.

Tuck, A. F., Watson, R. T., Condon, E.P., Margitan, J. J. and Toon, O. B. (1989). The planning and execution of ER-2 and DC-8 aircraft flights over Antarctica, August and September 1987, *J. Geophys. Res.*, **94**, 11181–11222.

Tuck, A. F., Brune, W. H. and Hipskind, R. S. (1997). Airborne Southern Hemisphere Ozone Experiment/Measurements for Assessing the Effects of Stratospheric Aircraft (ASHOE/MAESA): A road map. *J. Geophys. Res.*, **102**, 3901–3905.

van Loon, H. and Jenne, R. L. (1973). Zonal harmonic standing waves, *J. Geophys. Res.*, **78**, 21, 4463–4471.

Vaughan, G. and Price, K., D. (1991). On the relation between total ozone and meteorology, *Q. J. R. Meteorol. Soc.*, **117,** 1281–1298.

Waugh, D. W. (1997). Elliptical diagnostics of stratospheric polar vortices *Q. J. R. Meteorol. Soc.*, **123,** 1725–1748.

Waugh, D. W., Sisson, J. M. and Karoly, D. J. (1998). Predictive skill of an NWP system in the southern lower stratosphere, *Q. J. R. Meteorol. Soc.*, **124,** 2181–2200.

Washington, W. M., and Parkinson, C. L. (1986). An introduction to three-dimensional climate modelling. University Science Books, 422 pp.